AO08: Long-Term Trend Analysis of the Impact of Aerosols on Climate

Candidate number: 313055
Supervisors: Dr. M. Christensen &
Dr R. G. Grainger
Word count: 3,436

Abstract

The recent release of long-term data sets of the global distribution of both aerosol and cloud properties, processed by the Optimal Retrieval of Aerosol and Cloud algorithm, and spanning from the early 2000s up until 2012, have allowed new investigations into the relationships between these properties. In particular, they enable the problem of how aerosols affect climate (represented by the cloud properties) to be addressed. This was done by first considering the data from eight specific locations, before expanding to look at it globally. Both the trends in individual variables and the Pearson correlation coefficients between the variables were used. In addition, the correlation between these variables and the El Niño Southern Oscillation and anthropogenic aerosol emissions were examined (quantified by the Multivariate ENSO Index and the MACCity inventory respectively). The findings suggest that the natural variability of the ENSO cycle plays a larger role in affecting these cloud properties than the anthropogenic emissions.

1 Introduction

In the latest report from the Intergovernmental Panel on Climate Change (IPCC), the effect of aerosols on the Earth's radiation budget was flagged as the factor with the greatest associated uncertainty, to the extent that it's unknown whether the net impact is positive or negative [8]. Reducing this uncertainty is important for developing more accurate climate change models.

Aerosols interact with radiation in two ways: directly, absorbing and reflecting radiation in their own right, and indirectly, via their effects on cloud properties. This report is primarily concerned with the second. It's important to note that the word 'aerosol' in this context has a much broader scope than in everyday language. An aerosol is any 'dispersion of fine solid particles or liquid droplets in a gas" [3], and not just the propellant in an aerosol canister. This includes natural aerosols such as sand or sea salt, and anthropogenic pollutants such as sulphates or alcohols.

The release of new long-term data processed by the Optimal Retrieval of Aerosol and Cloud (ORAC) algorithm, developed jointly at Oxford and the Rutherford Appleton Laboratory, allows long-term trends in aerosol properties to be studied, along with the cloud properties that they are affecting. The aim of this report is to try and ascertain exactly what those effects are, and to tease out how much of that effect is due to anthropogenic aerosol emission.

2 Data

2.1 Aerosol CCI Data

The aerosol CCI data comes from the broader Climate Change Initiative (CCI) run by the European Space Agency [1]. The aim of the initiative is to bring together data on global aerosol distributions collected by various satellite mounted instruments, and processed by groups across Europe. The data we used came from two different instruments, ATSR-2 (Along Track

Scanning Radiometer 2) and AATSR (Advanced Along Track Scanning Radiometer). Together these sensors collected data that spans from July 1995 up until 2012, with some overlap: the ATSR-2 data runs until June 2003, and AATSR starts in August 2002.

The aerosol properties were extracted from the raw satellite data using the ORAC algorithm [9]. The particular product we were interested in was the monthly average, which gives, for every month of the time period covered, the average of various aerosol related variables for that month. The spatial extent of the data is the whole globe divided into regions of $1^\circ \times 1^\circ$ of latitude and longitude. The ORAC data is limited, however, as it is only available from July 2003, after the period covered by ATSR-2.

2.2 Cloud CCI Data

The cloud CCI data also falls under the umbrella of the CCI. This branch of the project though is concerned with gathering together data on the global distribution of cloud properties, rather than aerosol properties. The data comes once again from ATSR-2 and AATSR, and is processed by the cloud component of the ORAC algorithm [6]. The cloud data in question covers the period from January 1997 through to December 2011, with a gap for all of 2000, 2001 and 2002. Again, we were concerned with the monthly averages for cloud properties in this interval. The cloud CCI data differs from the aerosol CCI data in that the spatial resolution of the cloud data is a grid with regions that are $0.5^\circ \times 0.5^\circ$ rather than 1°. The interest, however, often lay in comparing the aerosol and cloud data at the same location. So, a modified data set with a 1° resolution was usually worked with, obtained by taking the average of four adjacent boxes in the original set to create a new box.

2.3 MACCity

The MACCity data is an inventory of global anthropogenic emissions of certain chemical species that impact on the radiation budget, covering the period from 1960 up until 2020, and given monthly on a grid with a resolution of $0.5^\circ \times 0.5^\circ$. The species in question are: carbon monoxide (CO), black carbon (BC), organic carbon (OC), nitrogen oxides (NO_x), ammonia (NH_3), sulphur dioxide (SO_2), ethane and other higher alkanes, ethene and other higher alkenes, methanol and other alcohols, formaldehyde and other aldehydes, acetone and other ketones, and various aromatics. The name is a portmanteau of two different climate projects: Monitoring Atmospheric Composition and Climate (MACC), which ran from 2009-2011 and was concerned with monitoring global air quality and climate forcing; and megaCITY - Zoom for the ENvironment (CityZEN), a 2008-2011 EU-funded project launched to examine the impact of large cities on air quality and climate.

The MACCity inventory is itself based on previous Atmospheric Chemistry and Climate Model Intercomparison Project (ACCMIP) data, a reconstitution of historical emissions from 1850 to 2000. The ACCMIP data catalogues the anthropogenic emissions for every month in every tenth year of that period, given as a monthly average [5]. This was then extended beyond 2000 by using a Representative Concentration Pathway (RCP), which is a possible scenario of how emissions might evolve in the future, based on various factors such as estimates of population change and technological advances. The particular RCP used to create the MACCity inventory is RCP8.5, where the 8.5 refers to the projected value of the radiative forcing by 2100 [7]. RCP8.5 is a pathway that corresponds to a high emission rate. The years in between the decade years are filled in via linear interpolation, while taking into account the natural cycle [4].

2.4 Multivariate ENSO Index (MEI)

The MEI is a measure of the El Niño Southern Oscillation, an interannual weather cycle centred over the Pacific. Mostly associated with the temperature of an ocean current travelling from Indonesia to the West Coast of the Americas, the ENSO cycle has a much wider effect on climate, in particular on rainfall, air pressure and wind velocities. There are two broadly opposite ways

the ENSO cycle manifests itself, either as El Niño or La Niña. During El Niño, the ocean current in question is relatively warm across the central Pacific; in La Niña, the current is cold in that region. The MEI combines six different variables that track how strong the ENSO effect is in any given year. These are: sea surface temperature, air temperature, the zonal and meridional wind components (that is, the wind velocity directed along a line of latitude and longitude respectively), the pressure at sea level and the cloud fraction [2]. The MEI ranges between roughly -3 and +3, with positive values corresponding to El Niño years, and negative values to La Niña years. The MEI is calculated monthly, and data exists from January of 1950 up until the present.

3 Methodology

The first step was to look at the data for eight individual locations, chosen because of their association with changes in aerosol optical depth (AOD) due to natural or human sources. These locations were: Eyjafjallajökull, Lima, Los Angeles, Luanda, Mumbai, New York, Oxford and Shanghai. We then expanded our scope to look at the data on a global scale, to see how the patterns at these individual sites played into larger variations.

3.1 Individual Locations

3.1.1 Individual Variables

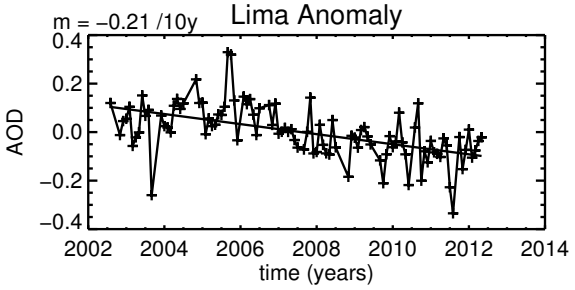

Figure 1: Time series for AOD anomaly in Lima, where m is the decadal trend

We focused our attention on four different variables. AOD, retrieved at 550 nm, measures how much sunlight is unable to reach the surface of the Earth due to the presence of the aerosol. AOD is a good indicator of how much aerosol is in the atmosphere at a particular location. Cloud optical thickness (COT) is a similar quantity, except that it indicates how much sunlight is blocked by cloud, rather than aerosol. The other two variables used were cloud fraction (CF), the fraction of the grid box in question occupied by cloud, and the cloud droplet effective radius (REF), which is a measure of the average radius of the droplets that make up the cloud. These variables were decided on because of their strong connection to the ability of clouds to reflect radiation, known as cloud albedo [10].

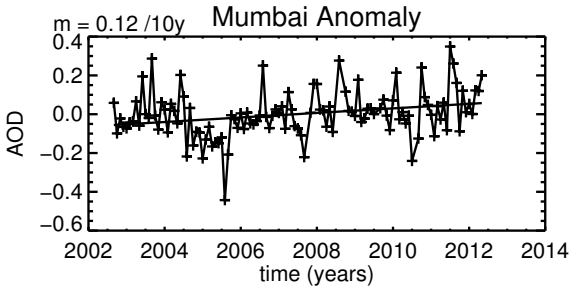

Figure 2: Time series for AOD anomaly in Mumbai, where m is the decadal trend

Two types of plot were constructed for each site and variable. The first was a plot of the monthly average of the variable in question, along with the line of best fit, calculated by minimising the chi-squared error statistic. The second (and more informative) type involved the deviation of each variable from the natural seasonal cycle, called the anomaly for short. AOD and other climate indices are subject to seasonal variation due to the natural weather cycle. So, in order to study any trends independent of this natural cycle, an estimate for the cycle was subtracted from each data point. The estimate for the annual cycle at each location came from taking the mean, for each month, of all the averages for that month throughout the time period. The anomaly was formed by subtracting the relevant long-term mean from each data point, before recalculating the line of best fit.

In order to decide which of these trends were

statistically significant, a two-tailed Student t-test was applied, along with a confidence threshold of 0.95. Only two of the locations had a change in AOD that was significant in this sense. These were Lima, where there was a decrease, and Mumbai, with an increase (Figures 1 and 2).

3.1.2 Residual Analysis

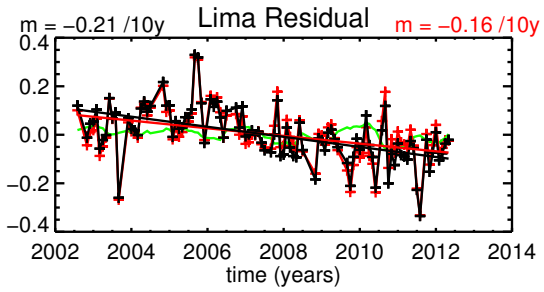

Figure 3: Time series for AOD anomaly, fit curve and residual curve in Lima, with the fit in green and the residual in red

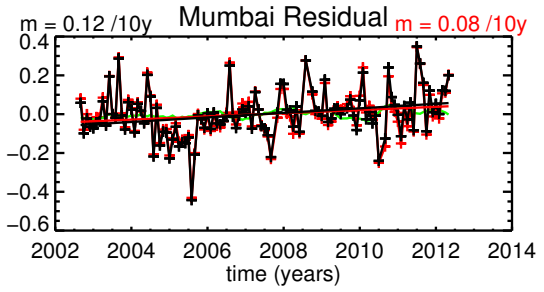

Figure 4: Time series for AOD anomaly, fit curve and residual curve in Mumbai, with the fit in green and the residual in red

A residual analysis was performed to determine whether the ENSO cycle might be able to explain the significant trends in AOD found at Lima and Mumbai. This would be expected particularly for Lima, which is located on the coast of the Pacific, where the ENSO effect is strongest.

The method of residuals involves first standardising the MEI index by subtracting the mean MEI value from each monthly MEI value, and then dividing by the standard deviation of the MEI. The gradient of the line of best fit is then calculated for the AOD anomaly against the standardised MEI. This gradient is multiplied by the standardised MEI, as a scaling factor, to generate a fit curve. The closer this fit curve is to the AOD anomaly curve, the more the variation in the anomaly is linked to the MEI. The residual curve is then just the difference between the original AOD anomaly and the fit.

Figures 3 and 4 are again the anomaly time series for AOD in Lima and Mumbai, but with the fit curve and the residual curve plotted on the same axes. The line of best fit for the trend in the residual is also shown. In both cases, the residual curve seems very close to the original curve, but there is nevertheless a change in the value of the trend by roughly a quarter in each case. This suggests that the ENSO cycle has a similar explanatory power in both cases.

3.2 Global Trends

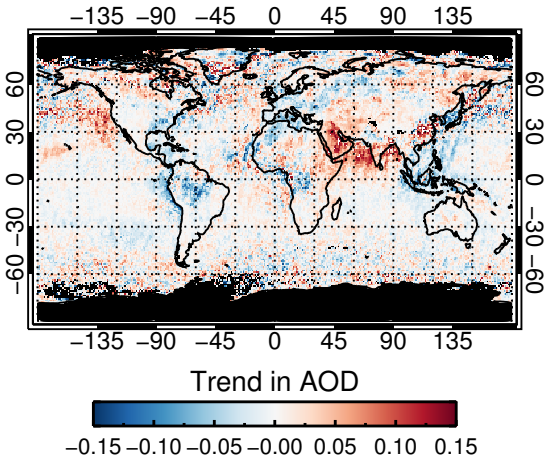

Figure 5: Global plot of the trend in AOD anomaly

3.2.1 Individual Variables

The global plots are generated in a similar way to the anomaly type plots above. The variable plotted is the slope of the line of best fit from the anomaly time series for each box. There is, however, a difference for the AOD anomaly, as detailed in the following subsection.

From the plot in Figure 5, it can be seen that the trends found in AOD over Lima and Mumbai are part of larger trends, off the west coasts of South America and India respectively.

3.2.2 Aerosol Retrievals

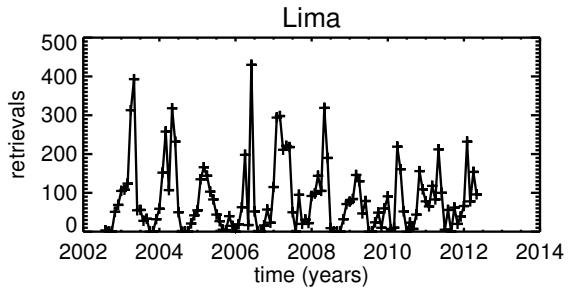

Figure 6: The number of retrievals going into the AOD averages for Lima

Figure 6 shows the number of retrievals that have gone into making the average for a particular month across the whole time period, for the grid box nearest Lima. The number of retrievals varies considerably, from values close to zero up to over four hundred. A priori, we would expect averages calculated using higher numbers of retrievals to be more accurate than those with lower numbers. Two plots were constructed in order to investigate this, and decide on a suitable threshold for the number of retrievals required to give a reliable average. These were contour plots of the monthly AOD average against the number of retrievals that went into making that average, as well as the uncertainty associated with each average against the number of retrievals. The data points used were restricted to those grid boxes contained between the Tropics, at 30°N and 30°S. The Tropics were used because of the sensitivity of the number of retrievals to the solar zenith angle, or the height of the sun in the sky. The lower the sun is in the sky, typically the fewer retrievals there will be. The solar zenith angle varies seasonally, as does the AOD. It follows that some correlation between the AOD value and the number of retrievals might be introduced via their joint dependence on the time of year. However, the seasonal variation of the zenith angle is minimal close to the Equator, or between the tropics.

Figure 7 contains the plot for AOD uncertainty against the number of retrievals. It shows that the range of uncertainties in AOD is high for very low numbers of retrievals, followed by a sharp drop in that range. This demonstrates, as might be expected, that the more retrievals that go into an average, the lower the uncertainty. This behaviour was repeated for the plot of the AOD averages against number of retrievals, which suggests that the large range in AOD for low numbers of retrievals is a result of skewed data resulting from that very low number of retrievals, rather than a reliable report of the actual AOD values. Based on these two plots, a threshold of 20 retrievals was decided upon, below which data points weren't deemed reliable. This threshold was chosen as a conservative estimate in order to discard the very high uncertainty data points, without losing too many from the overall data set. This threshold was implemented for all the global plots, excluding the unreliable data points from the estimates of the seasonal cycle, and the calculation of the slope of the line of best fit.

A similar analysis was attempted for the cloud properties, but no threshold could be determined. The analogous plots were all smeared out, as in Figure 8, showing no obvious correlation between variability in the cloud property and the number of retrievals.

3.2.3 Cross-Correlations

In order to assess where AOD and the cloud variables were possibly correlated, the Pearson correlation coefficient was used. It should be noted that these correlations were calculated using reduced data sets compared to the original ones. This is because the Pearson correlation is calculated based on pairs of data from the original set. So, for any particular month and location, a data point from the set for one variable could be included if and only if there was a corresponding data point for that same month and location in the other set. This wasn't always the case as the ranges of the aerosol and cloud data are different, and sometimes there simply isn't a value

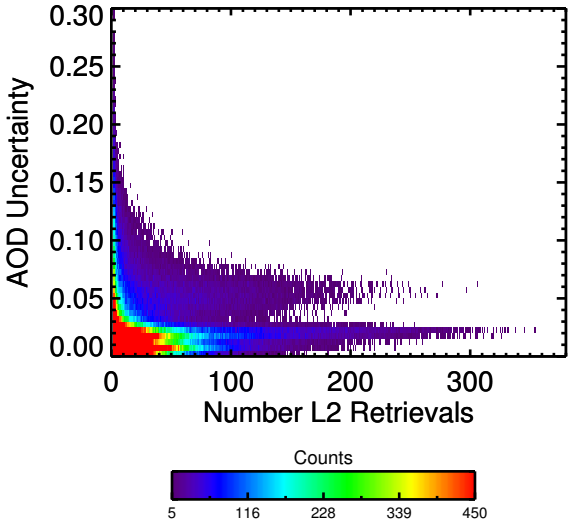

Figure 7: The uncertainty in AOD against number of retrievals for all grid boxes between 30°N and 30°S

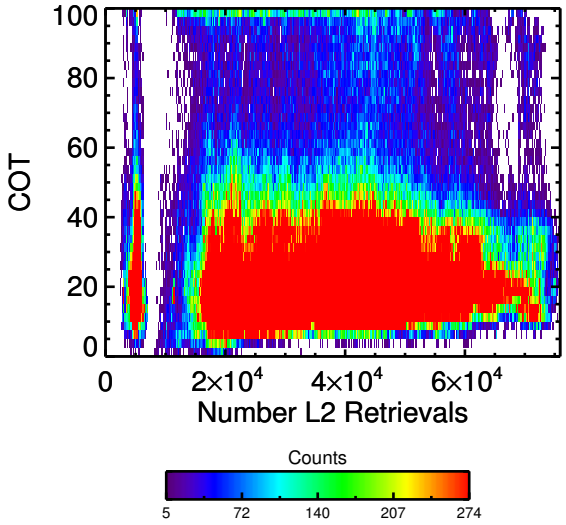

Figure 8: COT against number of retrievals for all grid boxes between 30°N and 30°S

for the monthly average for a particular month. This, together with the threshold for the number of retrievals, roughly halved the number of pairs of data points being used. The plot for the correlation between AOD and REF is shown above in Figure 9.

However, as before, the locations taken as significant were those where the confidence, as given by a two-tailed Student t-test, exceeded 0.95. Figure 10 above also shows the correlation between AOD and REF, but with all the locations where the correlation doesn't pass this threshold greyed out. This leaves the significant correlations fairly evenly spread out, with few broader regions where significant trends have clumped. Possible exceptions to this are off the west coast of Indonesia, the Gulf of Guinea, and the generalised positive correlation throughout the Pacific.

Table 1 summarises, for each cloud variable, the number of grid boxes with a positive correlation with AOD, the number with a negative correlation, and the number of those respectively which contain a significant trend.

3.2.4 ENSO Correlation

As the ENSO cycle plays such a large part in global climate, plots similar to above were constructed to investigate any correlation between the four variables chosen and the MEI. The most notable feature of these plots is that, for the cloud variables, there is a pattern of strong correlation repeated for all three, in the shape of a fork over the Pacific. This is a region of strong correlation over Indonesia that splits off towards the East, directed towards North and South America, as shown in Figure 11.

3.2.5 MACCity

More plots of a similar nature were constructed for the Pearson correlation between the variables and the MACCity emissions inventory. This was in order to try and quantify the anthropogenic influence on these quantities. Although the MACCity inventory is separated into different species, the sum of the different species was used.

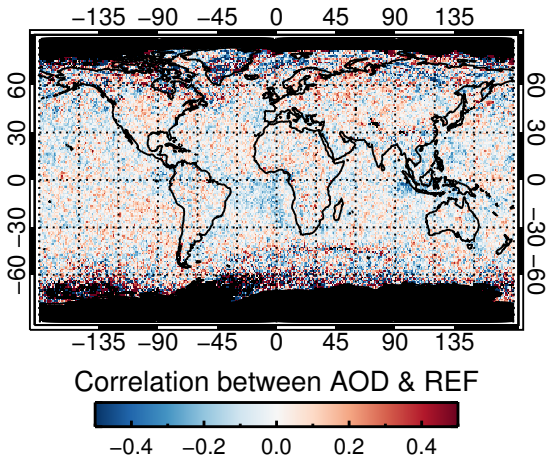

Figure 9: Global correlation between AOD and REF

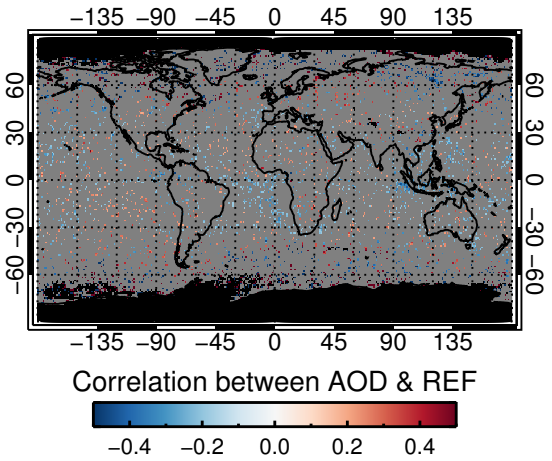

Figure 10: Global correlation between AOD and REF, where confidence in the correlation exceeds 0.95

4 Results

4.1 Twomey Hypothesis

One of the main ways that aerosols affect clouds is via the Twomey effect [10]. If the concentration of aerosol mixed in with a cloud increases, this will in general increase the number of cloud condensation nuclei (CCN) in the cloud. CCNs are particles that act as seeds for cloud droplets to form on. Increasing the concentration of CCNs in a cloud can either increase or decrease its albedo. Which of these dominates will depend on the thickness of the cloud. However, what should hold in both cases is that the average size of the droplets (and hence the REF) should decrease. This is because increasing the number of CCNs will increase the overall number of droplets, but the total volume of water contained by those droplets will be constant.

So, if we use the optical thickness of the aerosol as a proxy for the number of CCNs the aerosol provides, we should find that there is an inverse correlation between AOD and REF. Figure 9 shows the global distribution of this correlation. In terms of significance, there is a very slight bias towards negative correlation, with 6.5% of the positive grid boxes being significant, against 8.5% for the negative ones. This suggests a corroboration of the Twomey hypothesis.

In regions where the correlation is positive, the explanation could be the presence of very large, or "giant", CCNs [11]. Giant CCNs, such as sea salt, prevent smaller aerosols from activating as CCNs, meaning that even though the aerosol concentration in a cloud may be increasing, the CCN concentration may not be.

4.2 Anthropogenic Influence

Our method to quantify the anthropogenic influence was to use the MACCity inventory. Figure 12 of the correlation between emissions and REF shows that in general the correlation coefficient is very low, as is typical for these plots: less than 0.3. This suggests that the anthropogenic influence resulting from these emissions is in general fairly low. The regions over the ocean that show some correlation rather than none correspond to the emissions for major shipping routes.

5 Conclusion

The aim of this project was to investigate the effect of aerosols on climate, primarily via their interactions with various cloud properties. The evidence seems to suggest that anthropogenic emissions have a smaller impact on the radiation budget than natural cycles, such as ENSO.

There are two obvious paths future research

	Number of grid boxes that:			
Correlation between AOD and:	Have positive correlation	Have positive correlation and are significant	Have negative correlation	Have negative correlation and are significant
REF	24,371	1590 ($\approx$ 6.5%)	28,988	2487 ($\approx$ 8.6%)
COT	26,046	2267 ($\approx$ 8.7%)	27,313	1686 ($\approx$ 6.2%)
CF	36,555	6,329 ($\approx$ 17.3%)	16,804	1,069 ($\approx$ 6.3%)

Table 1: Sign and significances of the correlations in all grid boxes for AOD and the cloud properties

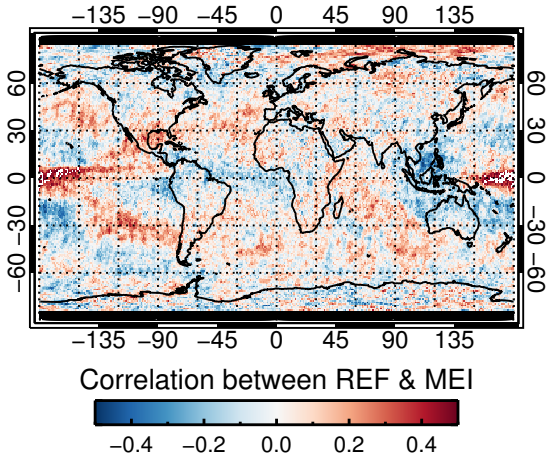

Figure 11: Global correlation between REF and MEI

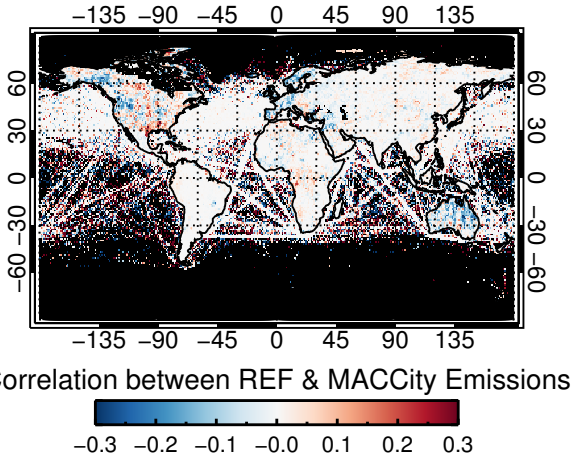

Figure 12: Global plot of the correlation between the total MACCity emissions inventory and REF

could take. One is to refine the work done here, by improving on some of the methods. For example, the MACCity inventory used was the simple sum of all the different species. The units for MACCity are kg/m^2/s though, and it's not clear that mass is the relevant property here. It has no direct relationship to CCN, or on the optical properties of the species. Using mol/m^2/s might be more informative. The second path would be to build on this work by considering how the solar energy reflected by clouds has also changed over time. Long-term satellite data does exist for this, and the possible correlations between it, AOD, and the other cloud variables, would help to clarify the role of aerosols in the radiation budget.

Finally, as the wealth of satellite data increases, applying these methods to data sets that cover longer periods should reveal insights missed here.

Acknowledgements

My greatest thanks go, of course, to my supervisors, Matt and Don. I have also benefited from the help of the others who work at AOPP, namely: Charlotte Birch, Elisa Carboni, Anu Dudhia, Cat Hayer, Greg McGarragh, Adam Povey, Simon Proud, Ben Reed, Lucy Ventress and Tony Vincent.

References

[1] http://www.esa-aerosol-cci.org/?q=overview.

[2] *Monitoring ENSO in COADS with a seasonally adjusted principal component index*. University of Oklahoma, Norman, OK., 1993.

[3] I. Colbeck, editor. *Physical and Chemical Properties of Aerosols*. Blackie Academic and Professional, 1998.

[4] C. Granier, B. Bessagnet, T. Bond, A. D'Angiola, H. Denier van der Gon, G. J. Frost, A. Heil, J. W. Kaiser, S. Kinne, Z. Klimont, S. Kloster, J.-F. Lamarque, C. Liousse, T. Masui, F. Meleux, A. Mieville, T. Ohara, J.-C. Raut, K. Riahi, M. G. Schultz, S. J. Smith, A. Thompson, J. Aardenne, G. R. Werf, and D. P. Vuuren. Evolution of anthropogenic and biomass burning emissions of air pollutants at global and regional scales during the 1980–2010 period. *Climatic Change*, 109(1):163–190, 2011.

[5] J.-F. Lamarque, T. C. Bond, V. Eyring, C. Granier, A. Heil, Z. Klimont, D. Lee, C. Liousse, A. Mieville, B. Owen, M. G. Schultz, D. Shindell, S. J. Smith, E. Stehfest, J. Van Aardenne, O. R. Cooper, M. Kainuma, N. Mahowald, J. R. McConnell, V. Naik, K. Riahi, and D. P. van Vuuren. Historical (1850-2000) gridded anthropogenic and biomass burning emissions of reactive gases and aerosols: methodology and application. *Atmospheric Chemistry and Physics*, 10(15):7017–7039, 2010.

[6] C. A. Poulsen, R. Siddans, G. E. Thomas, A. M. Sayer, R. G. Grainger, E. Campmany, S. M. Dean, C. Arnold, and P. D. Watts. Cloud retrievals from satellite data using optimal estimation: evaluation and application to ATSR. *Atmospheric Measurement Techniques*, 5(8):1889–1910, 2012.

[7] K. Riahi, S. Rao, V. Krey, C. Cho, V. Chirkov, G. Fischer, G. Kindermann, N. Nakicenovic, and P. Rafaj. RCP 8.5—A scenario of comparatively high greenhouse gas emissions. *Climatic Change*, 109(1):33–57, 2011.

[8] Core Writing Team, R.K. Pachauri, and L.A. Meyer. Climate change 2014: Synthesis report. contribution of working groups i, ii and iii to the fifth assessment report of the intergovernmental panel on climate change. Technical report, IPCC, Geneva, Switzerland, 2014.

[9] G. E. Thomas, C. A. Poulsen, A. M. Sayer, S. H. Marsh, S. M. Dean, E. Carboni, R. Siddans, R. G. Grainger, and B. N. Lawrence. The GRAPE aerosol retrieval algorithm. *Atmospheric Measurement Techniques*, 2(2):679–701, 2009.

[10] S. Twomey. The influence of pollution on the shortwave albedo of clouds. *Journal of the Atmospheric Sciences*, 34(7):1149–1152, 1977.

[11] T. Yuan, Z. Li, R. Zhang, and J. Fan. Increase of cloud droplet size with aerosol optical depth: An observation and modeling study. *Journal of Geophysical Research*, 113(D4), 2008.